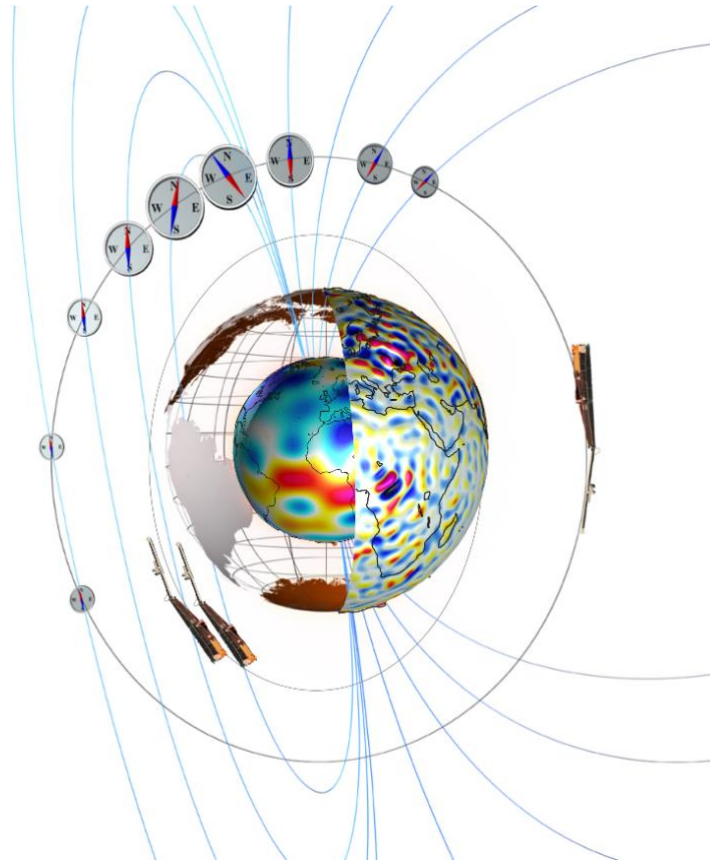




Swarm-AEBS Description of the Processing Algorithm



Doc. no: SW-DS-GFZ-GS-001, Rev: 6, Nov 2 2020

Prepared:

Guram Kervalishvili

Date 02 Nov 2020

Scientist

Checked:

Claudia Stolle

Date 02 Nov 2020

Team Leader

Prepared:

Jan Rauberg

Date 02 Nov 2020

Computer scientist

Approved:

Kirsti Kauristie

Date 02 Nov 2020

Group Leader

© GFZ, Germany, 2020. Proprietary and intellectual rights of GFZ, Germany are involved in the subject-matter of this material and all manufacturing, reproduction, use, disclosure, and sales rights pertaining to such subject-matter are expressly reserved. This material is submitted for a specific purpose as agreed in writing, and the recipient by accepting this material agrees that this material will not be used, copied, or reproduced in whole or in part nor its contents (or any part thereof) revealed in any manner or to any third party, except own staff, to meet the purpose for which it was submitted and subject to the terms of the written agreement.

Record of Changes

Reason	Description	Rev	Date
Initial vers.	Released.	1 dA	27 Jun 2018
Reference document list update	Section 2.2: the list from 21 to 32 and from 35 to 37 have been finalised.	1 dB	19 Mar 2019
Updated input from DTU	Section 4.1: text has been updated and two new figures have been added.	1 dC	20 Mar 2019
Updated input from DTU	Document text has been updated and corrected with minor changes.	1 dD	19 Sep 2019
Updated input from FMI	Text has been updated and corrected with minor changes on pages 7 (Sect. 2.1), 13, and 23. The document name, [AD-1] and [AD-2] have been updated.	1 dE	10 Oct 2019
Signature		1	10 Oct 2019
Input from DISC	Doc. No has changed from SW-DS-GFZ-GS-001_1-2_AEBS_DPA to SW-DS-GFZ-GS-001.	2 dA	21 Oct 2019
Signature		2	22 Oct 2019
Updated input from FMI	Section 5 has been updated with two new subsections: "Quality flagging of PBS and PBL" (Sect. 5.2) and "Occasional gaps in LPS when plotted according to latitude" (Sect. 5.3)	3 dA	24 Feb 2020
Signature		3	24 Feb 2020
Updated input from FMI	Title page has been updated	4 dA	20 Mar 2020
Signature		4	24 Mar 2020
Updated in response to Swarm AEBS discussions after the Final presentations	Description of the different mappings between Swarm and ionosphere used in the three methods added (Sects. 3.1 and 3.2). Descriptions added by Kirsti Kauristie	5 dA	21 Sep 2020
Signature		5	28 Sep 2020
Corrections after DISC validation	Correction to formula 4.1-2: Weight matrix W added. Modifications done by Kirsti Kauristie.	6 dA	30 Oct 2020

Reason	Description	Rev	Date
Signature		6	02 Nov 2020

Table of Contents

1	Introduction.....	7
1.1	Scope and applicability.....	7
2	Applicable and Reference Documentation	7
2.1	Applicable Documents	7
2.2	Reference Documents.....	7
2.3	Abbreviations	10
3	Scientific Background	12
3.1	Auroral electrojet: the line current method	12
3.2	Auroral electrojet: the SECS method	13
3.3	Auroral oval boundaries: the FAC method	14
4	Algorithms Description.....	15
4.1	Auroral electrojet: the line current method	15
4.2	Auroral electrojet: the SECS method	18
4.2.1	Mathematical description	18
4.2.1.1	Peak and boundary identification.....	21
4.2.2	Processing overview.....	21
4.2.2.1	Module 1: download and read Swarm data	22
4.2.2.2	Module 2: find approximate auroral oval crossings	22
4.2.2.3	Module 3: determine AEJ latitude profiles for the oval crossings	22
4.2.2.4	Module 4: determine AEJ peaks and boundaries for the latitude profiles	23
4.2.2.5	Module 5: save AEJ data	23
4.3	Auroral oval boundaries: the FAC method	23
4.3.1	Mathematical description	23
4.3.2	Processing overview.....	25
4.3.2.1	Module 1: read configuration file.....	26
4.3.2.2	Module 2: data pre-processing.....	26
4.3.2.3	Module 3: finding the auroral equatorial boundary	27
4.3.2.4	Module 4: finding the auroral poleward boundary.....	27
4.3.2.5	Module 5: saving of Swarm AOB data	27
5	Description of the output data	28
5.1	Output time span	28
5.2	Quality flagging of PBS and PBL	28

5.3 Occasional gaps in LPS when plotted according to latitude 29

List of Figures

Figure 3.1.1 Sketch of the geometry used in the Line Current method 12

Figure 4.1.1 Sketch of the geometry used in the Line Current method. 15

Figure 4.1.2 Sketch of the magnetic field caused by a line current “out of the plane” 17

Figure 4.2.1 Left: curl-free (CF) 1-D SECS and associated FACs for the case $d\theta_0 = 0$. Right: divergence-free (DF) 1-D SECS. The plots are reproduced from [RD-10]..... 18

Figure 4.2.2 Ionospheric sheet current density in the quasi-dipole frame..... 21

Figure 4.3.1 Two examples of auroral boundaries derived from high-latitude FAC measurements of Swarm A 24

Figure 4.3.2 Flowchart representing the processing (yellow arrows) and data (red arrows) flows of the AOB algorithm..... 26

1 Introduction

1.1 Scope and applicability

This document comprises the Swarm Level 2 (L2) Swarm-AEBS Description of the Processing Algorithm (DPA) document for the *Swarm Data, Innovation and Science Cluster* (Swarm DISC) consortium in response to the requirements of [AD-1]. Swarm-AEBS includes the following data products [AD-2]:

- AEJxLPL_2F – Latitude profiles of Westward Electrojet (WEJ) and Eastward Electrojet (EEJ) ionospheric sheet current densities determined using the Line Current method;
- AEJxLPS_2F – Latitude profiles of ionospheric sheet and radial current densities determined using the Spherical Elementary Current Systems method;
- AEJxPBL_2F – Auroral Electrojet Peaks and Boundaries determined using the Line Current method;
- AEJxPBS_2F – Auroral Electrojet Peaks, Boundaries and the maximum ground magnetic disturbance determined using the Spherical Elementary Current Systems (SECS) method;
- AOBxFAC_2F – Auroral Oval Boundaries (AOB) determined using the Field-Aligned Current (FAC) method.

The Swarm-AEBS Product Definition document [AD-2] is available in the SVN folder: https://smart-svn.spacecenter.dk/svn/smart/SwarmDISC/DISC_Projects/ITT1_2_Swarm_AEBS/Deliverables/.

Current or updated version of this document is available in the SVN folder: https://smart-svn.spacecenter.dk/svn/smart/SwarmDISC/DISC_Projects/ITT1_2_Swarm_AEBS/Deliverables/.

2 Applicable and Reference Documentation

2.1 Applicable Documents

The following documents are applicable to the definitions within this document.

[AD-1] SW-OF-FMI-GS-112_1-2_AEBS_Proposal, Proposal for Swarm DISC ITT 1.2, Swarm-AEBS – Auroral Electrojet and auroral Boundaries estimated from Swarm observations.

[AD-2] SW-DS-DTU-GS-003_1-2_AEBS_PDD, Swarm-AEBS Product Definition Document (PDD).

2.2 Reference Documents

The following documents contain supporting and background information to be taken into account during the activities specified within this document.

[RD-1] Olsen, N. (1996), A new tool for determining ionospheric currents from magnetic satellite data, *Geophys. Res. Lett.* 23, pp. 3635-3638, doi: 10.1029/96GL02896.

[RD-2] Olsen, N., Moretto, T., and Friis-Christensen, E. (2002), New approaches to explore the Earth's magnetic field, *Journal of Geodynamics* 33, pp. 29–41, doi: 10.1016/S0264-3707(01)00052-7.

[RD-3] Ritter, P., Viljanen, A., Lühr, H., Amm O., and Olsen, N. (2003), Ionospheric currents from CHAMP magnetic field data comparison with ground based measurements. In: Reigber C., Lühr H., Schwintzer P. (eds) *First CHAMP mission results for gravity, magnetic and atmospheric studies*. Springer, Berlin, pp .347–352, doi: 10.1007/978-3-540-38366-6_50.

- [RD-4] Ritter, P., Lühr, H., Viljanen, A., Amm, O., Pulkkinen, A., and Sillanpää, I. (2004), Ionospheric currents estimated simultaneously from CHAMP satellite and image ground-based magnetic field measurements: a statistical study at auroral latitudes. *Ann Geophys* 22, pp. 417–430, doi: 10.5194/angeo-22-417-2004.
- [RD-5] Aakjaer, C. D., Olsen, N., and Finlay, C. C. (2016), Determining polar ionospheric electrojet currents from Swarm satellite constellation magnetic data, *Earth Planets Space* 68, pp. 140, doi: 10.1186/s40623-016-0509-y.
- [RD-6] Aakjaer, C. D. (2017), Investigating the polar electrojet using Swarm satellite magnetic data, PhD, Technical University of Denmark.
- [RD-7] Alken, P. and Maus, S. (2007), Spatio-temporal characterization of the equatorial electrojet from CHAMP, Ørsted, and SAC-C satellite magnetic measurements, *Journal of Geophysical Research* 112, A09305, doi: 10.1029/2007JA012524.
- [RD-8] Alken, P., Maus, S., Vigneron, P., Sirol, O., and Hulot, G. (2013), Swarm SCARF equatorial electric field inversion chain, *Earth, Planets and Space* 65, pp. 1309–1317, doi: 10.5047/eps.2013.09.008
- [RD-9] Vanhamäki, H., Amm, O., and Viljanen, A. (2003), 1-dimensional upward continuation of the ground magnetic field disturbance using spherical elementary current systems, *Earth Planets Space* 55, pp. 613-625, doi: 10.1186/BF03352468.
- [RD-10] Juusola, L., Amm, O., and Viljanen, A. (2006), One-dimensional spherical elementary current systems and their use for determining ionospheric currents from satellite measurements, *Earth Planet Space* 58, pp. 667–678, doi: 10.1186/BF03351964.
- [RD-11] Juusola, L., Amm, O., Kauristie, K., and Viljanen, A. (2007), A model for estimating the relation between the Hall to Pedersen conductance ratio and ground magnetic data derived from CHAMP satellite statistics, *Ann. Geophys.* 25, pp. 721-736, doi: 10.5194/angeo-25-721-2007.
- [RD-12] Juusola, L., Kauristie, K., Amm, O., and Ritter, P. (2009), Statistical dependence of auroral ionospheric currents on solar wind and geomagnetic parameters from 5 years of CHAMP satellite data, *Ann. Geophys.* 27, pp. 1005-1017, doi: 10.5194/angeo-27-1005-2009.
- [RD-13] Vanhamäki, H., Amm, O., Kauristie, K., and Stolle, C. (2014), Exploiting synergies between Swarm and Cluster, Summary Report of Part 1, ESA report SWCL-SST-SRP1(2,CCN), May 5, 2014.
- [RD-14] Amm, O., Vanhamäki, H., Kauristie, K., Stolle, C., Christiansen, F., Haagmans, R., Masson, A., Taylor, M. G. G. T., Foberghagen, R., and Escoubet, C. P. (2015), A method to derive maps of ionospheric conductances, currents, and convection from the Swarm multisatellite mission, *J. Geophys. Res. Space Physics* 120, pp. 3263-3282, doi: 10.1002/2014JA020154.
- [RD-15] Juusola L., Kauristie, K., Vanhamäki, H., Aikio, A. T., and van de Kamp, M. (2016), Comparison of auroral ionospheric and field-aligned currents derived from Swarm and ground magnetic field measurements, *J. Geophys. Res.* 121, pp. 9256-9283, doi: 10.1002/2016JA022961.
- [RD-16] Juusola L., Archer, W. E., Kauristie, K., Burchill, J. K., Vanhamäki, H., Aikio, A. T. (2016), Ionospheric Conductances and Currents of a Morning-Sector Auroral Arc From Swarm-A Electric and Magnetic Field Measurements, *Geophys. Res. Lett.* 43, doi: 10.1002/2016GL070248.
- [RD-17] Amm, O. (1997), Ionospheric elementary current systems in spherical coordinates and their application, *J. Geomagn. Geoelectr.* 49, pp. 947-955, doi: 10.5636/jgg.49.947

- [RD-18] Amm, O. and Viljanen, A. (1999), Ionospheric disturbance magnetic field continuation from the ground to ionosphere using spherical elementary current systems, *Earth Planets Space* 51, pp. 431-440, doi: 10.1186/BF03352247.
- [RD-19] Richmond, A. D. (1995), Ionospheric Electrodynamics Using Magnetic Apex Coordinates, *J. Geomagn. Geoelectr.* 47, pp. 191-212, doi: 10.5636/jgg.47.191, 1995.
- [RD-20] Emmert, J.T., Richmond, A.D., and Drob, D.P. (2010), A computationally compact representation of magnetic-apex and quasi-dipole coordinates with smooth base vectors, *J. Geophys. Res.* 115, A08322, doi: 10.1029/2010JA015326.
- [RD-21] Feldstein, Y.I. (1963), Some Problems Concerning the Morphology of Auroras and Magnetic Disturbances at High Latitudes, *Geomagnetism and Aeronomy* 3, 183-195.
- [RD-22] Feldstein, Y. I., Isaev, S. I., and Lebedinsky, A. L. (1969), Phenomenology and morphology of aurorae, *Ann. Int. Quiet Sun Year*, 4, pp. 311–348.
- [RD-23] Akasofu, S.-I. (1966), The auroral oval, the auroral substorm and their relations with the internal structure of the magnetosphere, *Planet. Space Sci.*, 14, pp. 587–595.
- [RD-24] Frey, H. U. (2007), Localized aurora beyond the auroral oval, *Rev. Geo-phys.* 45, RG1003, doi: 10.1029/2005RG000174.
- [RD-25] Kauristie, K., Weygand, J., Pulkkinen, T. I., Murphree, J. S., and Newell, P. T. (1999), Size of the auroral oval: UV ovals and precipitation boundaries compared, *J. Geophys. Res.* 104, pp. 2321–2331.
- [RD-26] Pinnock, M. and Rodger, A. S. (2000) On determining the noon polar cap boundary from SuperDARN HF radar backscatter characteristics, *Ann. Geophys.* 18, pp. 1523–1530, doi: 10.1007/s00585-001-1523-2.
- [RD-27] Moen, J., Lockwood, M., Oksavik, K., Carlson, H. C., Denig, W. F., van Eyken, A. P., and McCrea, I. W. (2004), The dynamics and relationships of precipitation, temperature and convection boundaries in the dayside auroral ionosphere, *Ann. Geophys.* 22, pp. 1973–1987, doi: 10.5194/angeo-22-1973-2004.
- [RD-28] Aikio, A. T., Pitkänen, T., Kozlovsky, A., and Amm, O. (2006), Method to locate the polar cap boundary in the nightside ionosphere and application to a substorm event, *Ann. Geophys.* 24, pp. 1905–1917, doi: 10.5194/angeo-24-1905-2006.
- [RD-29] Newell, P. T., Meng, C.-I., and Lyons, K. M. (1996), Suppression of discrete aurorae by sunlight, *Nature* 381, pp. 766–767.
- [RD-30] Wang, H., Lühr, H., and Ma, S. Y. (2005), Solar zenith angle and merging electric field control of field-aligned currents: A statistical study of the Southern Hemisphere, *J. Geophys. Res.* 110, A03306, doi: 10.1029/2004JA010530.
- [RD-31] Newell, P. T., Liou, K., Sotirelis, T., and Meng, C.-I. (2001) Polar Ultraviolet Imager observations of global auroral power as a function of polar cap size and magnetotail stretching, *J. Geophys. Res.* 106, pp. 5895–5905, doi: 10.1029/2000JA003034.
- [RD-32] Østgaard, N., Mende, S. B., Frey, H. U., Sigwarth, J. B., Aasnes, A., and Weygand, J. (2007), Auroral conjugacy studies based on global imaging, *J. Atmos. Sol.-Terr. Phys.* 69, pp. 249–255, 2007.

- [RD-33] Xiong, C., Lühr, H., Wang, H., and Johnsen, M. G. (2014), Determining the boundaries of the auroral oval from CHAMP field-aligned current signatures – Part 1, *Ann. Geophys.* 32, pp. 609-622, doi: 10.5194/angeo-32-609-2014.
- [RD-34] Xiong, C. and Lühr, H. (2014), An empirical model of the auroral oval derived from CHAMP field-aligned current signatures – Part 2, *Ann. Geophys.* 32, pp. 623-631, doi: 10.5194/angeo-32-623-2014.
- [RD-35] Arfken, G.B. and Weber, H.J. (1995), *Mathematical Methods for Physicists*, Academic Press, New York.
- [RD-36] Fukushima, N. (1976), Generalized theorem for no ground magnetic effect of vertical currents connected with Pedersen currents in the uniform-conductivity ionosphere, *Rep. Ionos. Space Res. Japan.* 30, pp. 35–40.
- [RD-37] Press, W.H., Teukolsky, S.A., Vetterling, W.T., and B.P. Flannery (1992), *Numerical Recipes*, 2 nd ed, Cambridge Univ. Press, New York.

2.3 Abbreviations

Acronym or abbreviation	Description
AEBS	Auroral Electrojet and auroral Boundaries estimated from Swarm observations
AOB	Auroral Oval Boundaries
CHAMP	CHALLENGING Minisatellite Payload, https://www.gfz-potsdam.de/champ/
CF	Curl Free
DF	Divergence Free
DISC	The Data, Innovation and Science Cluster
DPA	Description of the Processing Algorithm (document)
EEJ	Eastward Electrojet
FAC	Field-Aligned Current
FMI	Finnish Meteorological Institute, Helsinki, FI
GEO	Geocentric coordinates (lat, lon, alt)
GFZ	The Helmholtz Centre Potsdam - GFZ German Research Centre for Geosciences, DE
LEO	Low Earth Orbit
L1b	Level 1b (satellite data)
L2	Level 2 (satellite data)
lat	latitude
MLat	Magnetic latitude

MLT	Magnetic Local Time
QD	Quasi-Dipole coordinate system
SECS	Spherical Elementary Current Systems
SPH	Spherical geographic coordinates (r, phi, theta)
SVN	SVN Repository with server located at DTU. Presently, the following URLs apply: https://smart-svn.spacecenter.dk/svn/smart/SwarmDISC/DISC_Projects/ITT1_2_Swarm_AEBS/
SVD	Singular Value Decomposition
SW	Software
Swarm	Constellation of 3 ESA satellites, https://earth.esa.int/web/guest/missions/esa-operational-eo-missions/swarm
TBD	To Be Defined
UT	Universal Time
WEJ	Westward Electrojet

3 Scientific Background

3.1 Auroral electrojet: the line current method

The line-current method was developed more than 20 years ago by Olsen [RD-1] and applied to data from the satellites Magsat [RD-1], POGO [RD-2], CHAMP [RD-3] [RD-4] and Swarm [RD-5] [RD-6] to determine latitudinal profiles of the horizontal sheet current density in the polar ionosphere describing the Auroral Electrojets. The same technique has also been used to estimate the current profile of the Equatorial Electrojet using CHAMP and Swarm satellite observations [RD-7] and is used on a routine basis in the Level-2 processing chain that yields the Swarm equatorial electric field (EEF) data product [RD-8].

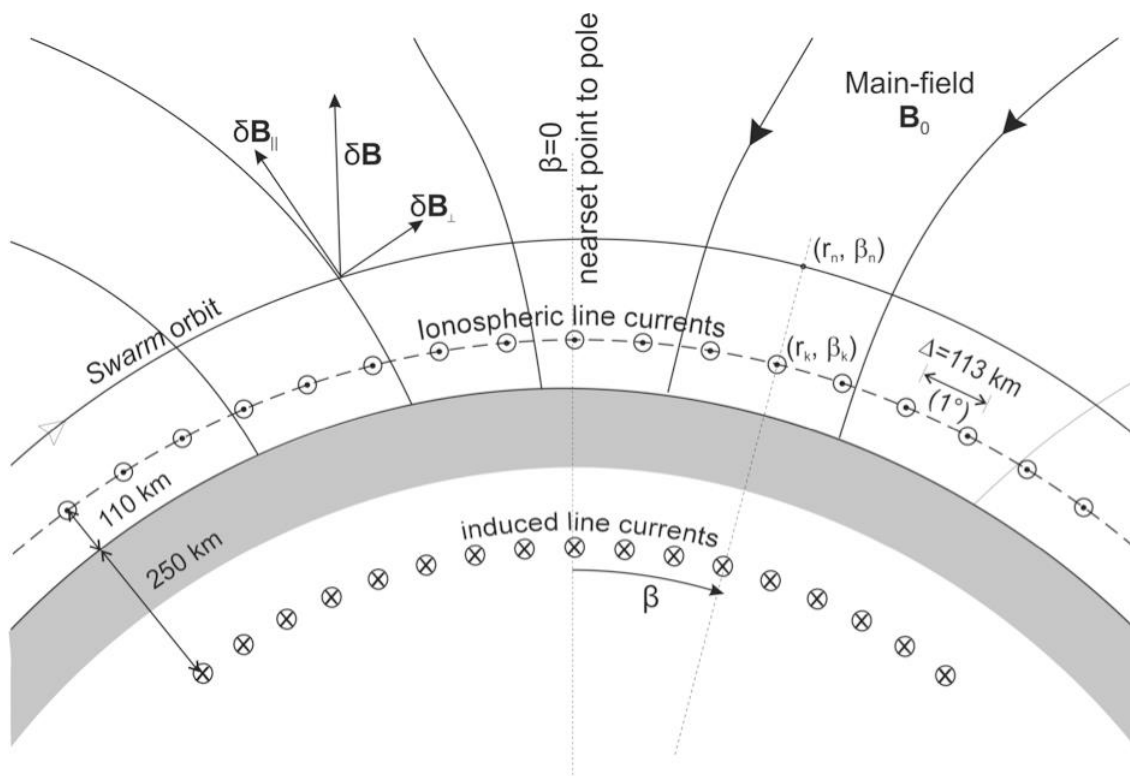


Figure 3.1.1 Sketch of the geometry used in the Line Current method: The auroral electrojets are described by a series of line-currents located at 110 km altitude and separated by 113 km in latitude.

We approximate the ionospheric sheet current density by a series of line-currents placed at 110 km altitude in the ionospheric E-layer, directed parallel to equal latitudes in QD coordinates and separated in horizontal (along-track) direction by $\Delta=113$ km (corresponding to 1°). The geometry of the model is shown in Figure 3.1.1. The magnetic field due to ionospheric E-layer currents is a Laplacian potential field at satellite altitude, and thus the strength of the magnetic field signature, and the spatial structure of the ionospheric currents that cause these magnetic variations, depend on the distance to the measurements. Determining the ionospheric current profile from Swarm magnetic field observations on an orbit-by-orbit basis yields time series of ionospheric current latitudinal profiles for a certain local time (which is slowly changing, due to the orbital drift of the satellite), and separately for Northern and Southern polar regions. In total, each orbit senses four crossings of the auroral zones, thus allowing for estimation of four current profiles (two in the Northern and two in the Southern hemisphere). Time series of the strength and location of polar cap currents

and AEJs are estimated from observed magnetic field variations along orbital parts by solving a linear inverse problem. The strengths and locations of AEJs are given at ionospheric level (altitude 110 km). The ionospheric footprints of Swarm satellites are determined with radial mapping.

3.2 Auroral electrojet: the SECS method

There are two major constituents to magnetic field perturbations at high latitudes: (1) horizontal electric currents flowing in a relatively thin layer in the ionospheric E-region (at an altitude of about 110 km) and (2) field-aligned currents (FACs) flowing parallel to the geomagnetic field lines between the E-region and the magnetosphere. The horizontal currents are typically modelled as sheet currents on a spherical surface with a radius of $R_E + 110$ km ($R_E =$ Earth radius). This horizontal ionospheric sheet current density can be separated into two components: the curl-free (CF) part, connected to the FACs such that it closes the regions of upward and downward FAC, and the divergence-free (DF) part, forming a rotational current that closes within the ionospheric current sheet. Ground-based magnetometers can only detect the DF currents, which are generally called equivalent currents. The dominant features of equivalent currents are the Auroral Electrojets (AEJs): the eastward electrojet (EEJ) in the dusk sector auroral oval and the westward electrojet (WEJ) around the midnight and in the dawn sector oval. Occasionally, especially in the pre-midnight sector, both electrojets can be observed at the same time, one located poleward of the other. Unlike ground magnetometers, a Low Earth Orbit (LEO) satellite measuring above the ionospheric current sheet detects the magnetic field signature not only from the DF currents but also from the CF currents (including FACs).

The one-dimensional Spherical Elementary Current Systems (1-D SECS) method was originally developed for the purpose of extracting latitude profiles of the DF current density from meridional chains of ground magnetometers [RD-9]. [RD-10] adapted the method for the derivation of DF, CF, and FAC current densities from latitude profiles of the vector magnetic field measured by a LEO satellite at auroral latitudes. Because such measurements do not provide information on longitudinal gradients, the method assumes these to be negligible (1-D assumption). As a result, the DF current only has an east component in the chosen coordinate system (e.g., geographic or magnetic) and the horizontal CF current has a south component. The method is routinely applied to determine electrojet profiles from ground-based IMAGE magnetometer data (<http://space.fmi.fi/image/>), and has been extensively applied to CHAMP satellite measurements [RD-11] [RD-12].

Recently, the SECS method was optimized for Swarm [RD-13] [RD-14] [RD-15] [RD-16]. This included determining the optimal spatial resolution with which the method can be applied without resorting to heavy regularization, improving the DF current density result by fitting the field-aligned component of the magnetic field signature instead of the radial one, and assessing the effect of the induced telluric currents. The latitude profiles of the DF current density derived separately for each Swarm satellite using the 1-D SECS method were validated against latitude-longitude maps of the DF current derived from IMAGE using the 2-D SECS method, developed by [RD-17] and [RD-18]. The more general 2-D SECS method makes no assumptions about the longitudinal gradients. The comparison showed excellent agreement for the east component of the ionospheric DF current density derived from Swarm and IMAGE, indicating that even when the strict 1-D condition is not fully applicable, the 1-D SECS method can still reliably describe the large-scale electrojet current.

Of course, the performance of the 1-D SECS method depends on the selection of the direction in which the longitudinal gradients are assumed to vanish (1-D coordinate system). The satellite orbit limits this selection, because sufficient latitude coverage needs to be retained. The Swarm-IMAGE comparison used geographic coordinates, which are almost equivalent to geomagnetic coordinates in the IMAGE area. Globally, the most straightforward choice would be magnetic coordinates, such as the Quasi Dipole (QD) [RD-19] [RD-20].

Optimization of the 1-D coordinate system for each auroral region crossing would be possible (e.g., [RD-11]), but a fixed coordinate system would be more robust in automatic production. Furthermore, as the large-scale electrojets are typically aligned along constant magnetic latitudes, the benefit of the more complicated analysis might not be significant.

The strengths and locations of the auroral electrojets vary in time, which is good to keep in mind when applying the SECS method where the currents are assumed to be stationary during the oval crossing (lasting typically ~6 mins). The time variations in electrojets induce telluric currents in the conducting ground and seawater. Below the ionospheric current sheet, the magnetic field of the induced telluric currents typically weakens the vertical field component of the ionospheric currents but strengthens the horizontal component. Above the ionospheric sheet the magnetic field of the telluric currents weakens all components of the magnetic field signature of the ionospheric DF currents. Because of this difference, separating the internal telluric and external ionospheric contribution to the disturbance magnetic field is fairly straightforward on the ground but complicated at LEO. Luckily, unlike on the ground, at LEO the effect of telluric currents appears to be significant only for very strong westward electrojets [RD-15]. The strengths and locations of auroral electrojet are given at ionospheric level (altitude 110 km). The ionospheric footprints of Swarm satellites are determined with mapping along the geomagnetic field line.

3.3 Auroral oval boundaries: the FAC method

The best-known aurora features are the northern and southern auroral ovals [RD-21] [RD-22] [RD-23] that are the regions in the ionosphere receiving the main part of the magnetospheric particle precipitation. Viewed from space with a global imager, the aurora appears as diffuse, continuous, luminous bands that surround both geomagnetic poles at ionospheric altitudes [RD-24]. The dynamics of the auroral oval is related to the prevailing geomagnetic activity, and the exact locations of the boundaries depend on the precipitating particles energy as well as the magnetospheric electric and magnetic fields [RD-25].

The boundaries of the auroral oval can be determined locally by ground-based observations such as radars [RD-26] [RD-27] [RD-28] or low-altitude satellite observations [RD-29] [RD-30], while optical imagers from high-altitude satellites can provide an instantaneous global view of the auroral oval [RD-31] [RD-32]. By using magnetic field observations from the CHAMP satellite, in [RD-33] a method was developed for detecting auroral boundaries from small-scale FAC signatures. In a statistical analysis they demonstrated the reliability of their approach, and an empirical model [RD-34] for predicting auroral boundaries has also been constructed based on 10-year dataset of boundaries derived from CHAMP. Therefore, polar LEO satellites like CHAMP and Swarm provide magnetic observations essentially in North-South direction, allowing for a determination not only of the strength and current profiles of the AEJs but also of its location and width. The Swarm satellites, with its unique constellation and high-resolution on-board magnetometers, will definitely provide precise and excellent global coverage of the auroral boundaries.

4 Algorithms Description

4.1 Auroral electrojet: the line current method

We approximate the ionospheric sheet current density by a series of line-currents placed at 110 km altitude in the ionospheric E-layer, directed parallel to equal latitudes in QD coordinates and separated in horizontal (along-track) direction by $\Delta=113$ km (corresponding to 1°). The geometry of the model is shown in Figure 3.1.1 and Figure 4.1.1.

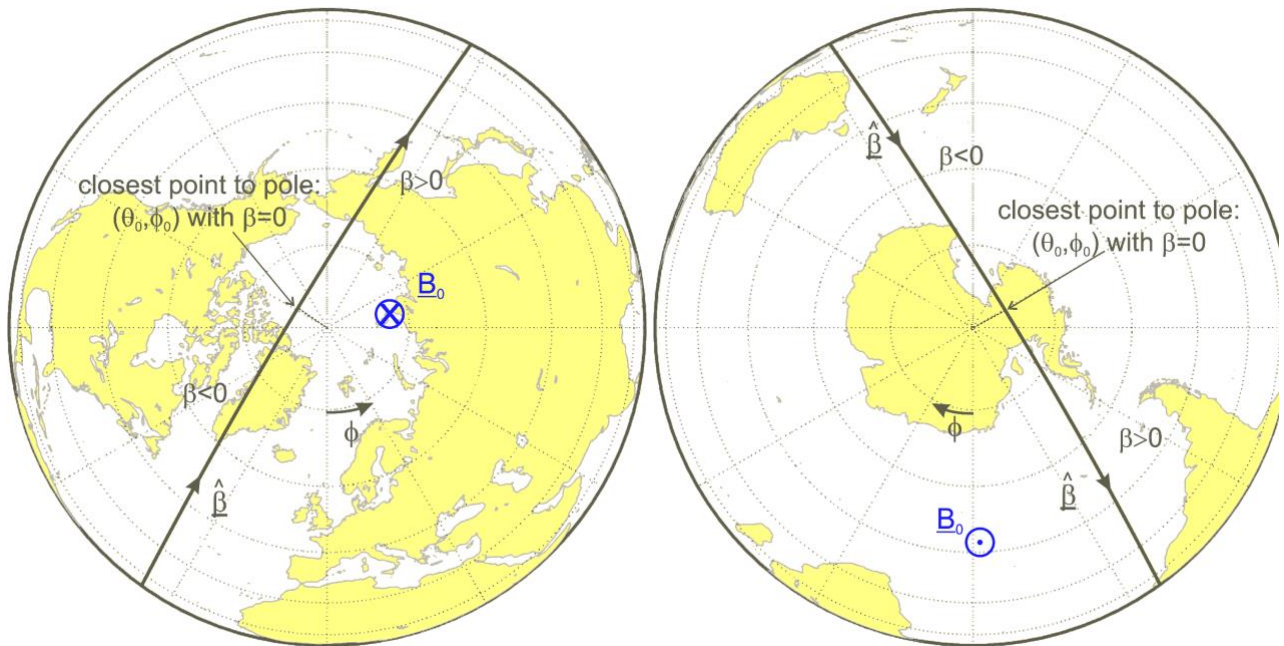


Figure 4.1.1 Sketch of the geometry used in the Line Current method.

The described approach relies on Swarm measurements of the magnetic field intensity at 1 Hz sampling, provided as Swarm L1b product MAGx_LR_1b. Only magnetic field intensity is required, which means that the algorithm is independent of possible issues with the attitude data, or with processing of the vector data (i.e. robust regarding failures in L1b processing). In addition, use of the field disturbance in the direction of ambient magnetic field minimizes unwanted magnetic field contamination FACs, the magnetic field perturbations of which are in general much stronger compared to those of the ionospheric horizontal currents comprising the AEJs. Our algorithm is therefore very robust and suited for automatic product generation. However, the algorithm needs the magnetic residuals, i.e. the differences between Swarm observations minus model values (describing contributions from the core, crust and magnetosphere) at the same time and location as the measurements. We use the CHAOS geomagnetic model (latest version, presently CHAOS-6) for calculating the core, lithospheric and large-scale magnetospheric contributions.

The algorithm involves the following steps:

- 1) Calculate magnetic model vector values \mathbf{B}_{mod} , including core, lithospheric and large-scale magnetospheric (and Earth-induced) contributions, for the time and position of the Swarm satellite observations;

- 2) Determine the geographic co-latitude θ_0 and longitude ϕ_0 of the satellite point closest to the geographic pole – this is done separately for processing the data in the Northern, resp. Southern Hemisphere;
- 3) Determine the orbital parameter β for each data point of the selected orbit part, using spherical trigonometry:

$$\cos \beta = \cos \theta_0 \cos \theta + \sin \theta_0 \sin \theta \cos(\phi - \phi_0), \quad \text{Eq. 4.1-1}$$

$\beta=0$ corresponds to the position θ_0, ϕ_0 . The sign of β is chosen such that locations from the ascending part of the orbit (corresponding to decreasing β) have negative sign of β while those of the descending part have positive values. See Figure 3.1.1 for details;

- 4) Calculate QD latitude, and units vector $\underline{\hat{\beta}} = (\beta_r = 0, \beta_\theta, \beta_\phi)$ of flight direction (assuming strictly horizontal flight direction, i.e. $\beta_r = 0$) and the unit vector $\underline{\hat{b}} = \frac{\mathbf{B}_{\text{mod}}}{|\mathbf{B}_{\text{mod}}|} = (b_r, b_\theta, b_\phi)$ of the ambient field direction for each observation point;
- 5) Select the data of each orbit (separately for the Northern and Southern Hemisphere) for which $-50^\circ < \beta < +50^\circ$. This yields N data points; Determine the model parameterization, the location of the $K=120$ line currents. Their “beta angle” are given by $\beta_k = [-59.5:1:59.5]$. (This step is independent on the actual data and can be done once for all orbits). The magnetic field vector, $\delta \underline{B}$, produced by a line current of strength I_k at position (r_k, β_k) at the satellite observation point (r_n, β_n) assuming the electrical currents are “out of the plane” as in Figure 4.1.2, is directed counter clockwise. Considering cylindrical coordinates (s, φ, z) , where the angle φ is counted as positive in the counter clockwise, this magnetic field can be written

$$\delta \underline{B} = \frac{\mu_0 I_k}{2\pi s} \underline{\hat{\varphi}}$$

Here $s = \sqrt{\xi^2 + \eta^2}$ with $\eta = r_k \sin(\beta_n - \beta_k)$, $\xi = r_n - r_k \cos(\beta_n - \beta_k)$, $r_k = a + 115$ km and $a = 6371$ km. Considering Cartesian coordinates (x, y) , where x points along the flight direction, i.e. in the direction of δB_H , and y points in the radial direction of δB_r , we have $x = s \cos \varphi$, $y = s \sin \varphi$. The unit vector is written as $\underline{\hat{\varphi}} = -\sin \varphi \underline{\hat{x}} + \cos \varphi \underline{\hat{y}}$, such that

$$\begin{aligned} \delta \underline{B} &= \frac{\mu_0 I_k}{2\pi s} \left[-\sin \varphi \underline{\hat{x}} + \cos \varphi \underline{\hat{y}} \right] \\ &= \frac{\mu_0 I_k}{2\pi s} \left[-\frac{\xi}{s} \underline{\hat{x}} + \frac{\eta}{s} \underline{\hat{y}} \right] \\ &= \frac{\mu_0 I_k}{2\pi \sqrt{\xi^2 + \eta^2}} \left[\frac{\eta}{\sqrt{\xi^2 + \eta^2}} \underline{\hat{y}} - \frac{\xi}{\sqrt{\xi^2 + \eta^2}} \underline{\hat{x}} \right] \\ &= \frac{\mu_0 I_k}{2\pi(\xi^2 + \eta^2)} \left[\eta \underline{\hat{y}} - \xi \underline{\hat{x}} \right] \end{aligned}$$

Consequently, the scalar disturbance field at position (r_n, β_n) is given by the scalar product with the unit vector in ambient magnetic field direction: $\delta F \approx \underline{\hat{b}} \cdot \delta \underline{B} = \delta B_H \underline{\hat{\beta}} \cdot \underline{\hat{b}} + \delta B_r b_r$ where

$$\begin{aligned} \delta B_H &= -I_k \frac{\mu_0}{2\pi} \frac{\xi}{\xi^2 + \eta^2} \\ \delta B_r &= I_k \frac{\mu_0}{2\pi} \frac{\eta}{\xi^2 + \eta^2} \end{aligned}$$

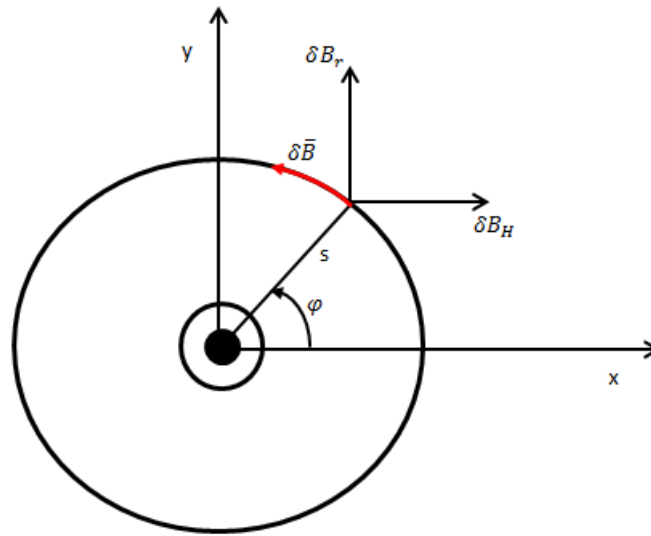


Figure 4.1.2 Sketch of the magnetic field caused by a line current “out of the plane”.

- 6) Thus the elements $g_{n,k}$ of the data kernel matrix \mathbf{G} are given by $g_{n,k} = \frac{\mu_0 \eta b_r - \xi (\hat{\beta} \cdot \hat{b})}{2\pi \xi^2 + \eta^2}$. Note that this is a slightly revised version of eqs. (1) and (3) of [RD-5] to account for ambient field direction that is not entirely in the orbital plane;
- 7) Determine the model regularisation matrices. We work with two regularisation matrices:
 - a. Minimisation of the second spatial derivative (curvature) of the line currents results in the first regularisation matrix Ω_1^{-1} with corresponding regularisation parameter α_1^2 ;
 - b. Minimisation of the line current strength at non-polar latitudes is realized by a second regularisation matrix Ω_2^{-1} with corresponding regularisation parameter α_2^2 . Ω_2^{-1} is a diagonal matrix with elements given by $\sin^4 \beta_k$;
- 8) Collecting the scalar anomaly $\Delta F_{obs} = \{\Delta F_n\}, n = 1 \dots N$ in the data vector \mathbf{d} and the model parameters (the strength J_k of the line K currents) in the model vector \mathbf{m} leads to the linear problem $\mathbf{d} = \mathbf{G}\mathbf{m}$;
- 9) The model vector \mathbf{m} (which contains the current strengths of the $K=120$ line currents) is estimated by solving the linear inverse problem

$$\mathbf{m} = (\mathbf{G}^T \mathbf{W} \mathbf{G} + \alpha_1^2 \Omega_1^{-1} + \alpha_2^2 \Omega_2^{-1})^{-1} \mathbf{G}^T \mathbf{W} \mathbf{d}. \quad \text{Eq. 4.1-2}$$

using Iteratively reweighted Least Squares with Huber weights (Huber parameter $c = 1.5$), collected in the diagonal data weight matrix \mathbf{W} .

- 10) Data residuals $\delta F = \Delta F_{obs} - \Delta F_{mod}$ are determined for each of the N data points, and the rms of the data misfit, $rms_{\delta F}$, is determined for each of the four orbital crossings (two on each side of the pole in each hemisphere, and for each hemisphere defined by $\beta > 0$ and $\beta < 0$, respectively) is calculated using the robust data weights w determined in the previous step. In a similar way we calculate the rms of the signal (from ΔF_{obs} instead of δF), rms_F , and from these two numbers the unitless confidence, $conf = 1 - rms_{\delta F}/rms_F$. This is a quantity between 0 (indicating no data fit) and 1 (indicating perfect data fit). The time instants assigned to $rms_{\delta F}$ and $conf$ is t_{qual} ;
- 11) The sheet current density J_{QD} (in units of A/km), is determined from the line current amplitudes by dividing the elements of the model vector \mathbf{m} (i.e. the line current strengths in units of A) by 0.111

km. In order to get the correct sign (positive in Eastward QD direction) the sign of x is reversed when $\beta_k > 0$ in the Northern Hemisphere, resp. when $\beta_k < 0$ in the Southern Hemisphere;

- 12) Horizontal sheet current density $\underline{J}_{geo} = (J_{geo,\theta}, J_{geo,\phi}) = J_{QD}(f_{1,\theta}, f_{1,\phi})$ in the geographic frame is determined using the unit vectors $\underline{f}_1 = (f_{1,\theta}\hat{\theta}, f_{1,\phi}\hat{\phi})$ of equal QD-longitude (cf. Fig. 1 of Richmond 1995).

4.2 Auroral electrojet: the SECS method

4.2.1 Mathematical description

The idea of the 1-D SECS method is to expand the co-latitude (θ) profile of the horizontal ionospheric sheet current density $\underline{J}(\theta)$ (unit: A/km) on a spherical surface with a radius $R_I = R_E + 110$ km ($R_E = 6371.2$ km) in terms of a set of CF and DF basis functions. FAC density $j(\theta)$ (unit: A/km²) is associated with the divergence of the CF SECS and assumed to flow radially. In the original formulation [RD-9] [RD-10], the CF system had a δ -function divergence (infinitely thin FAC sheet) and the DF system a δ -function curl at the co-latitude θ_0 , and uniform oppositely directed sources elsewhere. Figure 4.2.1 shows a sketch of such systems.

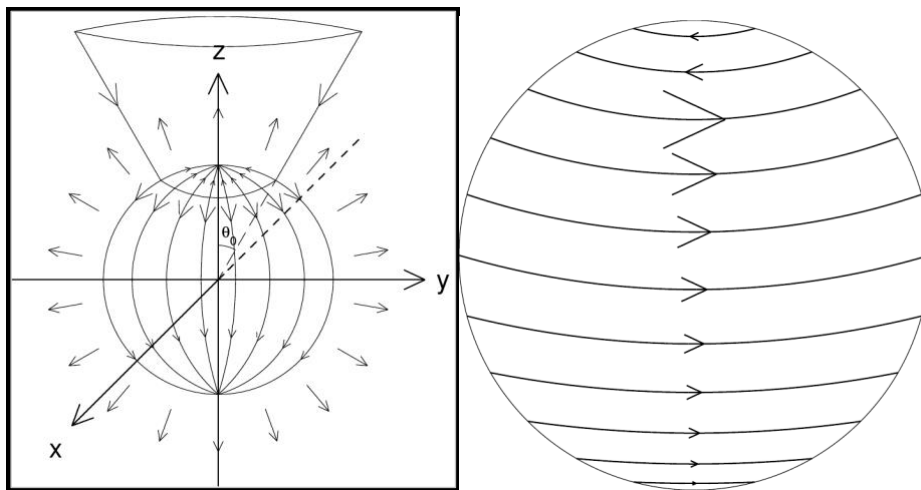


Figure 4.2.1 Left: curl-free (CF) 1-D SECS and associated FACs for the case $d\theta_0 = 0$. Right: divergence-free (DF) 1-D SECS. The plots are reproduced from [RD-10].

The FAC density was calculated by assuming that the sheet FAC was uniformly distributed over the latitude range between two neighbouring CF 1-D SECS elements. Some care needed to be taken with relative locations of θ_0 , measurement points, and the latitudes where the current densities were calculated, as locations too close to the δ -functions could result in numerical problems. Lately, this problem has been circumvented by slightly modifying the equations such that instead of a δ -function divergence or a curl, the CF system has a uniform divergence (FAC density) and the DF system a uniform curl between the co-latitudes $\theta_0 \pm d\theta_0/2$, and uniform and oppositely directed sources distributed across the entire sphere:

$$J_{\{CF,\theta\}}^{\{DF,\phi\}} = \begin{cases} \frac{I_{DF}^{CF}}{2R_I} \times \frac{-1+\cos\theta}{\sin\theta} = \frac{I_{DF}^{CF}}{2R_I} \times \tan\frac{\theta}{2} & \theta \leq \theta_0 - d\theta_0/2 \\ \frac{I_{DF}^{CF}}{2R_I} \times \frac{-1+\cos\theta}{\sin\theta} + \frac{I_{DF}^{CF}}{R_I} \times \frac{\cos(\theta_0-d\theta_0/2)-\cos\theta}{(\cos(\theta_0-d\theta_0/2)-\cos(\theta_0+d\theta_0/2))\sin\theta} & \theta_0 - d\theta_0/2 < \theta \leq \theta_0 + d\theta_0/2 \\ \frac{I_{DF}^{CF}}{2R_I} \times \frac{1+\cos\theta}{\sin\theta} = \frac{I_{DF}^{CF}}{2R_I} \times \cot\frac{\theta}{2} & \theta > \theta_0 + d\theta_0/2 \end{cases} \quad \text{Eq. 4.2-1}$$

$$j_{CF,r}(\theta) = \begin{cases} \frac{I_{CF}}{2R_I^2} & \theta \leq \theta_0 - d\theta_0/2 \\ \frac{I_{CF}}{2R_I^2} - \frac{I_{CF}}{R_I^2} \times \frac{1}{\cos(\theta_0 - d\theta_0/2) - \cos(\theta_0 + d\theta_0/2)} & \theta_0 - d\theta_0/2 < \theta \leq \theta_0 + d\theta_0/2 \\ \frac{I_{CF}}{2R_I^2} & \theta > \theta_0 + d\theta_0/2 \end{cases}$$

Here, I_{CF} and I_{DF} are the scaling factors of the elementary current systems. The subscripts r , θ , and ϕ refer to three orthogonal components that are positive in the radially upward, southward, and eastward directions, respectively.

The magnetic field of the CF 1-D SECS, modified from [RD-10], is:

$$B_{CF,\phi}(r, \theta) = \begin{cases} 0 & r < R_I \\ \left\{ \begin{array}{l} \frac{\mu_0 I_{CF}}{2r} \times \frac{1-\cos\theta}{\sin\theta} = \frac{\mu_0 I_{CF}}{2r} \times \tan\frac{\theta}{2} & \theta \leq \theta_0 - \frac{d\theta_0}{2} \\ \frac{\mu_0 I_{CF}}{2r} \times \frac{1-\cos\theta}{\sin\theta} - \frac{\mu_0 I_{CF}}{r} \frac{\cos(\theta_0 - d\theta_0/2) - \cos\theta}{(\cos(\theta_0 - d\theta_0/2) - \cos(\theta_0 + d\theta_0/2))\sin\theta} & \theta_0 - \frac{d\theta_0}{2} < \theta \leq \theta_0 + \frac{d\theta_0}{2} \\ \frac{\mu_0 I_{CF}}{2r} \times \frac{-1-\cos\theta}{\sin\theta} = -\frac{\mu_0 I_{CF}}{2r} \times \cot\frac{\theta}{2} & \theta > \theta_0 + \frac{d\theta_0}{2} \end{array} \right\} & r > R_I \end{cases} \quad \text{Eq. 4.2-2}$$

With the approximation $d\theta_0 = 0$ that simplifies computations, the magnetic field due to the divergence-free system is for all values of θ [RD-9]:

$$B_{DF,r}(r, \theta) = \begin{cases} \frac{\mu_0 I_{DF}}{2r} \sum_{l=1}^{\infty} \left(\frac{r}{R_I}\right)^l P_l(\cos\theta_0) P_l(\cos\theta) & r < R_I \\ \frac{\mu_0 I_{DF} R_I}{2r^2} \sum_{l=1}^{\infty} \left(\frac{R_I}{r}\right)^l P_l(\cos\theta_0) P_l(\cos\theta) & r > R_I \end{cases} \quad \text{Eq. 4.2-3}$$

$$B_{DF,\theta}(r, \theta) = \begin{cases} \frac{\mu_0 I_{DF}}{2r} \sum_{l=1}^{\infty} \left(\frac{r}{R_I}\right)^l \frac{1}{l} P_l(\cos\theta_0) P_l^1(\cos\theta) & r < R_I \\ -\frac{\mu_0 I_{DF} R_I}{2r^2} \sum_{l=1}^{\infty} \left(\frac{R_I}{r}\right)^l \frac{1}{l+1} P_l(\cos\theta_0) P_l^1(\cos\theta) & r > R_I \end{cases}$$

Here, P_l^m are associated Legendre functions [RD-35].

The scaling factors are determined by best fit of the SECS' magnetic field to the perturbation magnetic field, obtained as a residual between the measurement (\mathbf{B}) and a model background field (\mathbf{G}):

$$\begin{aligned} \delta B_r(r, \theta) &= B_r(r, \theta) - G_r(r, \theta) \\ \delta B_\theta(r, \theta) &= B_\theta(r, \theta) - G_\theta(r, \theta) \\ \delta B_\phi(r, \theta) &= B_\phi(r, \theta) - G_\phi(r, \theta) \end{aligned} \quad \text{Eq. 4.2-4}$$

The scaling factors $I_{CF}(\theta_0)$ are obtained by fitting δB_ϕ . For $I_{DF}(\theta_0)$, the best results are obtained by fitting the geomagnetic field-aligned component [RD-1] [RD-15]:

$$\delta B_{||} = \frac{\delta B_r \times G_r + \delta B_\theta \times G_\theta}{\sqrt{G_r^2 + G_\theta^2}} \quad \text{Eq. 4.2-5}$$

The corresponding DF 1-D SECS is similarly obtained:

$$B_{DF,||}(r, \theta) = \frac{B_{DF,r} \times G_r + B_{DF,\theta} \times G_\theta}{\sqrt{G_r^2 + G_\theta^2}} \quad \text{Eq. 4.2-6}$$

The fittings can be formulated as matrix operations:

$$\begin{aligned} [\delta B_{||}(r, \theta)] &= [M^{B_{DF,||}}(r, \theta, \theta_0)] \times [I_{DF}(\theta_0)] \\ [\delta B_\phi(r, \theta)] &= [M^{B_{CF,\phi}}(r, \theta, \theta_0)] \times [I_{CF}(\theta_0)] \\ [I_{DF}(\theta_0)] &= [M^{B_{DF,||}}(r, \theta, \theta_0)]^{-1} \times [\delta B_{||}(r, \theta)] \\ [I_{CF}(\theta_0)] &= [M^{B_{CF,\phi}}(r, \theta, \theta_0)]^{-1} \times [\delta B_\phi(r, \theta)] \end{aligned} \quad \text{Eq. 4.2-7}$$

Here, the notation M^B refers to the geometry factor of the SECS magnetic field, i.e., without the scaling factor, and the notation "[...]" means a matrix comprising all observation points (r, θ) and/or SECS poles (θ_0) . The ionospheric current density or fitted residual magnetic field can then be obtained at any location as:

$$\begin{aligned} [J_{DF,\phi}(\theta)] &= [M^{J_{DF,\phi}}(r, \theta, \theta_0)] \times [I_{DF}(\theta_0)] \\ [J_{CF,\theta}(\theta)] &= [M^{J_{CF,\theta}}(r, \theta, \theta_0)] \times [I_{CF}(\theta_0)] \\ [j_{CF,r}(\theta)] &= [M^{j_{CF,r}}(r, \theta, \theta_0)] \times [I_{CF}(\theta_0)] \\ [\delta B_{DF,r}(r, \theta)] &= [M^{B_{DF,r}}(r, \theta, \theta_0)] \times [I_{DF}(\theta_0)] \\ [\delta B_{DF,\theta}(r, \theta)] &= [M^{B_{DF,\theta}}(r, \theta, \theta_0)] \times [I_{DF}(\theta_0)] \\ [\delta B_{CF,\phi}(r, \theta)] &= [M^{B_{CF,\phi}}(r, \theta, \theta_0)] \times [I_{CF}(\theta_0)] \end{aligned} \quad \text{Eq. 4.2-8}$$

The SECS method does not require any assumptions about the ionospheric conductance. In particular, the conductance need *not* be assumed to be uniform, as was incorrectly stated in [RD-36].

When applying the SECS method, the spatial resolution of the ionospheric current density to be solved is determined by choosing the distances $d\theta_0$ between the poles (θ_0) of the elementary current systems. We use the singular value decomposition (SVD, [RD-37]) to solve the inversion problem of obtaining the SECS amplitudes by the best fit to the magnetic field measurements. SVD can be thought of as a representation of the involved matrix in terms of a set of eigenvectors and corresponding eigenvalues, organized in descending order. An ill-determined solution, which manifests itself as spurious current density values, can be improved by removing some of the smallest eigenvalues and corresponding vectors. A parameter called epsilon (ϵ) is used to describe this cut-off, such that any eigenvalues smaller than ϵ times the largest eigenvalue are not included in the solution. Ideally, ϵ should be given as small a value as possible as the effect of increasing ϵ is to produce smoother solutions. However, apart from adjusting ϵ , there is also another way of optimizing the problem: by adjusting the number of unknowns, i.e., changing the SECS grid resolution. Increasing the distances between the SECS poles basically has the same effect as increasing ϵ : both smooth the result. Adjusting the grid resolution has the advantage that the resulting spatial resolution is then known exactly.

While [RD-15] applied a vanishingly small ϵ , we found that for obtaining reasonably smooth current density profiles suitable for determining peak and boundary values, fairly dense grid spacing is better (1°). This required increasing ϵ to the value of 0.01.

4.2.1.1 Peak and boundary identification

Consider the ionospheric sheet current density (J) as a function of latitude (lat). Assume that J varies linearly between each grid point. To determine the location of the eastward and westward electrojet, apply the following steps:

- 1) Find sequences of positive (eastward) and negative (westward) current densities.
- 2) Calculate the total current across each sequence.
- 3) Eastward electrojet (EEJ) is defined to be located within the sequence of the largest positive current. Similarly, the westward electrojet (WEJ) is located within the sequence of the smallest negative current.

Figure 4.2.2 shows an example of EEJ and WEJ detection for an oval crossing with the above-described method.

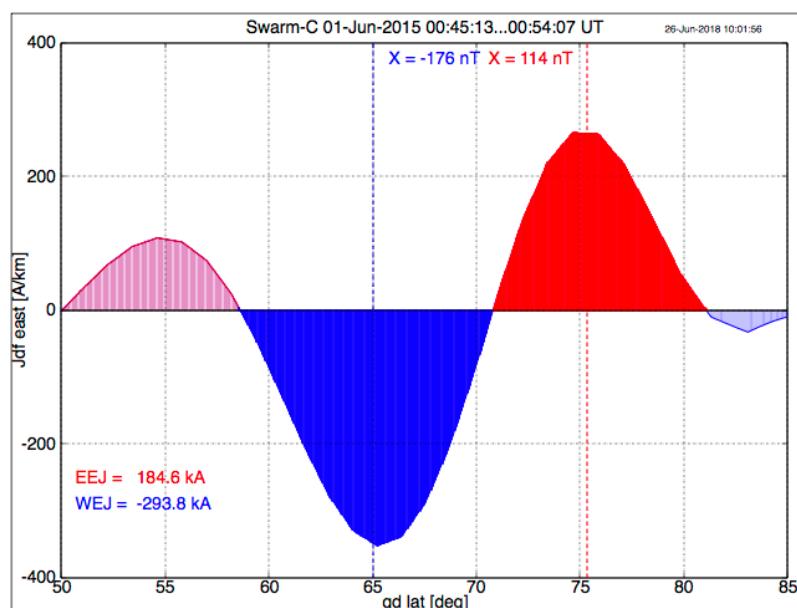


Figure 4.2.2 Ionospheric sheet current density in the quasi-dipole frame. Red indicates eastward current and blue shading westward current. Dark shading denotes the latitude range within which the electrojets are located. The total amplitudes are shown too. The dashed vertical lines show the location of the maximum (red) and minimum (blue) of the modelled northward ground magnetic field.

We note that we use the terms eastward and westward electrojet in a wider sense than usually in high-latitude ionospheric physics. It is more conventional to use EEJ and WEJ only for currents occurring at a certain local time and within a certain latitude range.

4.2.2 Processing overview

The expansion of Swarm 1 Hz magnetic field measurements in terms of DF and CF 1-D SECS requires coordinate transformations between several systems and mapping between different altitudes.

- 1) Swarm data are provided in spherical geographic coordinates as a function of universal time (UT).
- 2) Quasi-dipole (QD) mapping of the Swarm location to the ionospheric altitude is applied to define the points at which ionospheric current densities are determined.
- 3) The 1-D SECS output will be given at
 - a. Satellite locations (magnetic field fit).
 - b. Ionospheric footprints of the satellites at 110 km altitude (current density).

- c. Ground footprints of the satellites at 0 km altitude (ground magnetic field).
- 4) The available Apex library (<http://apexpy.readthedocs.io/en/latest/readme.html>) converts between geodetic and QD coordinates, maps between different altitudes along the geomagnetic field, and provides the magnetic local time (MLT).
- 5) The output will be provided in the natural 1-D (QD) as well as the geographic coordinates generally used for Swarm data.

The processing flow of the algorithm for Swarm AEJ-SECS consists of five main modules:

- 1) Module 1: download and read Swarm data (Sect. 4.2.2.1)
- 2) Module 2: find approximate auroral oval crossings (Sect. 4.2.2.2)
- 3) Module 3: determine AEJ latitude profiles for the oval crossings (Sect. 4.2.2.3)
- 4) Module 4: determine AEJ peaks and boundaries for the latitude profiles (Sect. 4.2.2.4)
- 5) Module 5: save AEJ data (Sect. 4.2.2.5)

4.2.2.1 *Module 1: download and read Swarm data*

- Download MAGx_LR_1B files and read data for a given satellite.
- Download VirES baseline data and read background geomagnetic field model values.
- Check input data quality and replace obviously false values by NaN.
- Calculate the residual magnetic field by subtracting the background field from Swarm recordings. As the background field is by models of core, crust and magnetospheric fields, we assume that the residual field is produced only by ionospheric currents.

4.2.2.2 *Module 2: find approximate auroral oval crossings*

Auroral oval crossings are assumed to occur within the QD latitude range 50 to 85 degrees in the northern hemisphere and similarly between -50 to -85 degrees in the southern hemisphere. This region is wide enough to cover all typical locations of auroral electrojets. The poleward limit is necessary to prevent computational problems that would be present if a SECS system were placed very close to the pole. At this stage, we do not care whether the Swarm orbit fully covers this latitude range or not. It often lacks the most poleward parts, but consequences are estimated when quality flags are determined. The SECS method works without problems in such cases too.

4.2.2.3 *Module 3: determine AEJ latitude profiles for the oval crossings*

To obtain the best benefit of the QD system, the SECS method is applied in a spherical geocentric system whose north pole is defined as follows:

- If Swarm is above the northern hemisphere then the SECS pole is equal to the QD north pole (magnetic latitude 90 deg).
- If Swarm is above the southern hemisphere then the SECS pole is the antipodal point of the QD south pole (magnetic latitude -90 deg).

The reason for the special treatment in the latter case is that the QD poles are not antipodal.

The precise QD coordinate system is not orthogonal, and vector transforms from other frames to QD do not preserve the magnitude. However, the SECS method requires a spherical frame, and it is also consistent to preserve vector magnitudes. Consequently, the transform from the geographic coordinate system to the SECS system is a rotation between two spherical geocentric frames.

The resolution of the 1-D SECS grid at 110 km altitude equals to the width of the CF 1-D SECS FAC sheets and is selected to be $d\theta_0 = 1^\circ$, requiring an SVD $\varepsilon = 0.01$. The SECS grid at latitudes $\{\theta_0\}$ is uniformly spaced by $d\theta_0$ between the minimum and maximum of θ_l as defined in Sect. 4.2.2.2.

The SECS method provides the ionospheric DF and CF sheet current densities and the radial current density related to the CF currents. Additionally, the ground magnetic field produced by the DF current is calculated. As a reminder, the CF sheet currents together with the associated radial currents do not produce any magnetic field below the ionosphere.

4.2.2.4 *Module 4: determine AEJ peaks and boundaries for the latitude profiles*

The location of the electrojets is determined as described in Sect. 4.2.1.1. In an ideal case, both EEJ and WEJ can be uniquely detected within the predefined latitude range. However, there are several cases in which one or two of them cannot be properly located. For example, Swarm does not always reach high QD latitudes and then the poleward boundary of the electrojet may be indefinite. The complete list of the quality flags is given in [AD-2].

4.2.2.5 *Module 5: save AEJ data*

The full list of output quantities from the SECS modelling is defined in [AD-2]. The locations (latitude, longitude) are expressed in the spherical geocentric system and in the QD system. As discussed in Sect. 4.2.2.3, SECS modelling is performed in a spherical system with its pole defined by the QD system. Consequently, the current densities attributed to QD points are not strictly speaking true QD vectors. However, since they are also given in the well-defined geographic system, it is possible to convert them to any other coordinate frame in further analysis.

4.3 Auroral oval boundaries: the FAC method

4.3.1 Mathematical description

Estimates of FACs (single satellite method) are routinely derived from the magnetic measurements of each Swarm spacecraft and provided as the L2 data product FACxTMS_2F. For determining the auroral boundaries, we used the small-scale (down to 15 km) FAC part of this data product. Larger scales are suppressed by subtracting 20 s averaged values, corresponding approximately to 150 km along Swarm orbits, as the auroral boundaries are more sharply detected from the small-scale FACs.

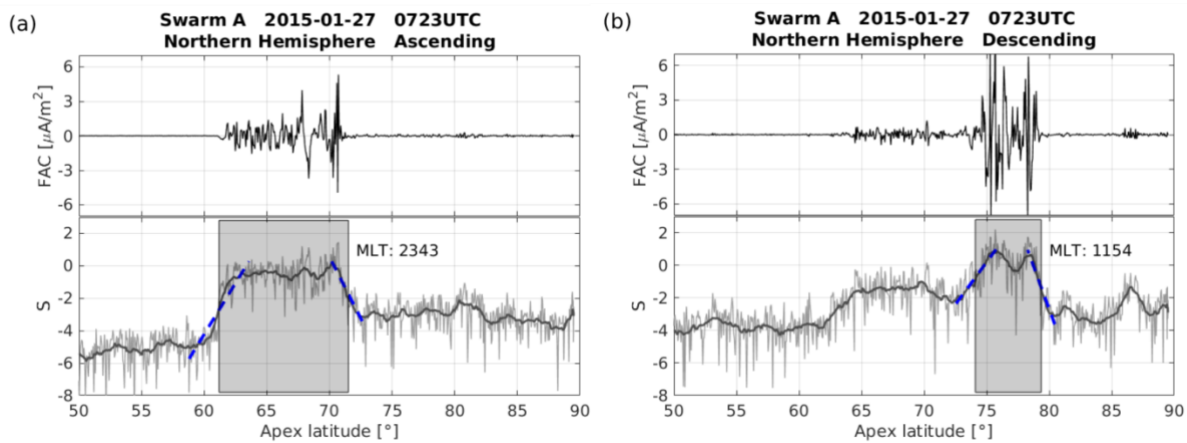


Figure 4.3.1 Two examples of auroral boundaries derived from high-latitude FAC measurements of Swarm A around 0723 UTC on 27 January 2015 for (a) ascending and (b) descending arcs. For each example, the top panel present the small-scale FACs and the bottom panel is the corresponding S curves for detecting auroral boundaries. In the bottom panel, the grey thin line indicates the variations of S value, as defined by Eq. 4.3-1, and the grey thick line is the 20 s averaged value of S . The blue dashed line is the linear part of S value with steep gradients, representing the equatorial and poleward boundaries, respectively, and the grey shadow area indicates the auroral oval derived by our approach.

Figure 4.3.1 (a) presents such an example of the small-scale FACs activity (top panel) at auroral latitudes on 27 January 2015 derived from Swarm A. We can see a well-defined latitude range, marked by high FAC intensity that we associate with the auroral oval. The magnetic QD latitude [RD-19] [RD-20] used here facilitates a mapping of FACs at satellite height along geomagnetic field lines down to the ionospheric E-layer (about 110 km altitude). Further, a variable S has been used to represent the FAC intensity, which is defined as:

$$S = \langle \log_{10} j_{\parallel}^2 \rangle_{20s}. \quad \text{Eq. 4.3-1}$$

Because of the wide range of variations encountered during a boundary crossing, we consider the logarithm of the squared current density (to avoid negative values in S). The FAC density, j_{\parallel} , is given in units of $\mu\text{A}\cdot\text{m}^{-2}$. We take averages over 20 s for the values of S . The latitude profiles of FACs and corresponding S values are then calculated individually along the four high-latitude segments (from $\pm 50^\circ$ QD latitude to the magnetic pole in both hemispheres) for each Swarm orbit. Data from these segments were surveyed subsequently by an automatic procedure to find the linear parts of the S curve with steep gradients. We start to check from the latitude of maximum S value to lower and higher latitudes for equatorward and poleward boundaries, respectively.

Taking the equatorward boundary as an example, we start with S_c representing the FAC density at the maximum S value of the considered orbital arc. S_c is compared with a reading S_E further equatorward. We step down S_E until the condition $S_c - S_E \geq 2$ is valid. Then a linear function S^* is used to fit the curve of S value over the latitude range from QD latitudes of S_c to S_E :

$$S^* = a \cdot S + b, \quad \text{Eq. 4.3-2}$$

where a and b are the linear fit slope and intercept, respectively, for describing the function S^* . In a next step we use the standard deviation, σ , to check the quality of the linear fit:

$$\sigma = \sqrt{\langle (S - S^*)^2 \rangle \Big|_C^E}, \quad \text{Eq. 4.3-3}$$

where the boundaries C and E represent the start and end point of the linear segment of S . If σ is larger than 0.25, we will move S_C to the next latitude data point. Otherwise, we consider the data from S_C to S_E as a good linear part. Subsequently, S_E is advanced to lower latitude until σ becomes larger than 0.25. To find the exact start and end point of this linear segment, the S_C to S_E will be further extended to their nearest inflexion point of the S curve. Then S_C is stepped forward until the two conditions are met again. This process continues until S_E has reached the lowest QD latitude (50°) of the considered orbital arc. From all accepted linear segments the steepest is selected for final consideration. At last, we choose from this segment the mid-point between S_C and S_E to represent the equatorial boundary of the auroral oval.

The same approach is applied to determine the polar boundary of the auroral oval, with the exception that S_E is moved until the highest QD latitude that Swarm can reach, to find the steepest linear segment that is used for boundary determination.

The bottom panel of Figure 4.3.1 (a) illustrates the detection procedure described above. The blue dashed lines indicate the linear part with steep gradients of S value at both equatorward and poleward, and the shadowed area indicates the derived auroral oval. Similarly, Figure 4.3.1 (b) presents the consecutive arc (descending node) of small-scale FACs observed by Swarm A.

4.3.2 Processing overview

The processing flow of the algorithm for Swarm AOB consists of five main modules (Figure 4.3.2):

- 1) Module 1: (Sect. 4.3.2.1)
- 2) Module 2: data pre-processing (Sect. 4.3.2.2)
- 3) Module 3: finding the auroral equatorial boundary (Sect. 4.3.2.3)
- 4) Module 4: finding the auroral poleward boundary (Sect. 4.3.2.4)
- 5) Module 5: saving of Swarm AOB data (Sect. 4.3.2.5)

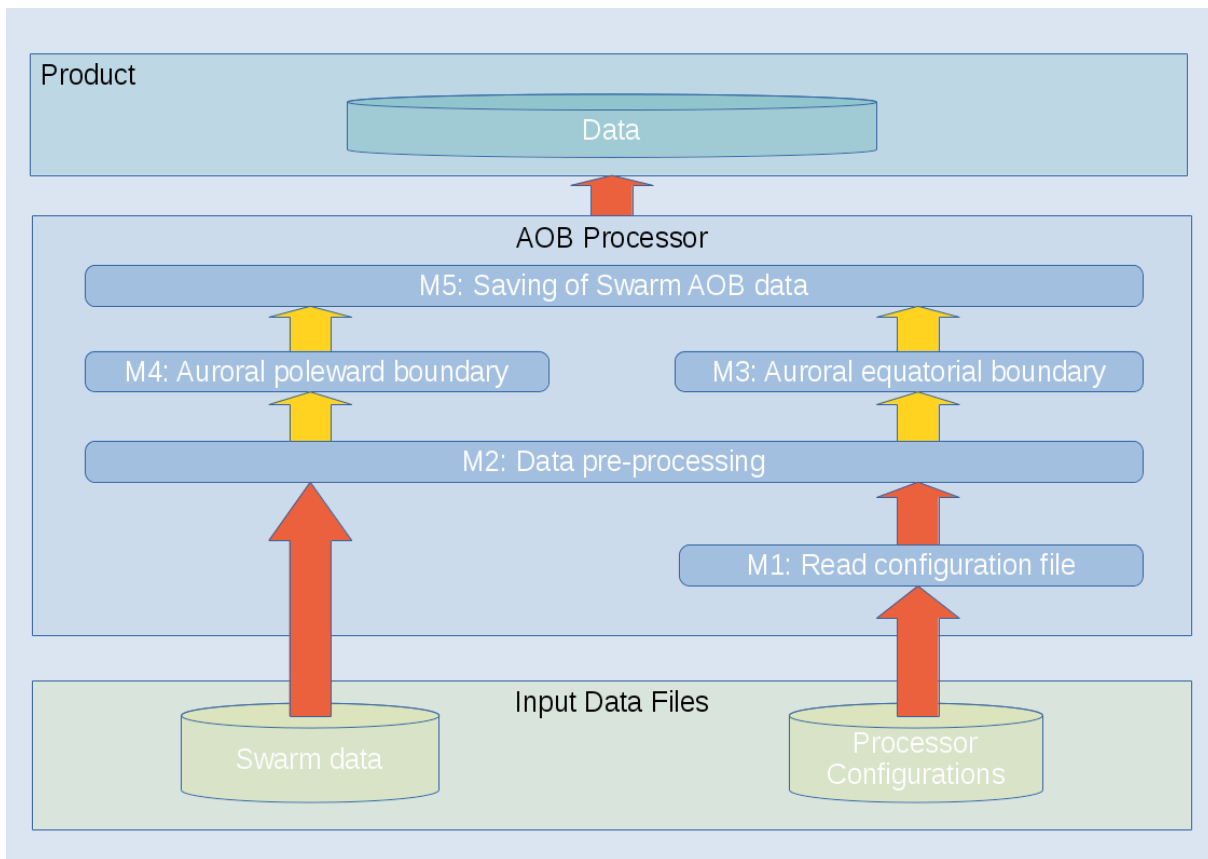


Figure 4.3.2 Flowchart representing the processing (yellow arrows) and data (red arrows) flows of the AOB algorithm.

4.3.2.1 *Module 1: read configuration file*

The following list describes the single processing steps in the module 1:

- Read configuration file for the given Swarm satellite
- Create and return an internal data structure as input for the other modules: **data-m1**

4.3.2.2 *Module 2: data pre-processing*

The following list describes the single processing steps in the module 2:

- Take over: **data-m1** (Sect. 4.3.2.1)
- Read input:
 - a. FAC data of the previous day
 - b. FAC data of the current day
- Combine the FAC data of the previous and current day
- Calculate the Magnetic Local Time (MLT) and Magnetic Latitude (MLat), i.e. QD latitude
- Divide the data into orbits and find out the high-latitude orbital arcs: $|\text{MLat}| > 50^\circ$
- For each high-latitude orbital arc, the FAC data are first filtered, to suppress the larger-scales FAC by subtracting 20 s averaged values
- The rest of small-scale FAC are converted to S value, which represents the intensity of FAC, averages over 20 s are taken for the values of S .

- Return all input variables, magnetic coordinates, and values of S as internal data structure: **data-m2**

4.3.2.3 *Module 3: finding the auroral equatorial boundary*

The following list describes the single processing steps in the module 3:

- Take over: **data-m2** (Sect. 4.3.2.2)
- Find the maximum S value of the considered orbital arc
- From the maximum value towards equatorward, find the linear part of S value with deepest slope
- The middle points of the linear part is then taken as the auroral equatorial boundary
- If no linear part of the S value is identified, the auroral equatorial boundary is recorded as *NaN* value
- Return time, location, and magnetic coordinates: **data-m3**

4.3.2.4 *Module 4: finding the auroral poleward boundary*

The following list describes the single processing steps in the module 4:

- Take over: **data-m2** (Sect. 4.3.2.2)
- From the maximum value towards poleward, find the linear part of S value with deepest slope
- The middle points of the linear part is then taken as the auroral poleward boundary
- If no linear part of the S value is identified, the auroral poleward boundary is recorded as *NaN* value
- Return time, location, and magnetic coordinates: **data-m4**

4.3.2.5 *Module 5: saving of Swarm AOB data*

The following list describes the single processing steps in the module 5:

- Take over: **data-m3** (Sect. 4.3.2.3)
- Take over: **data-m4** (Sect. 4.3.2.4)
- Save AOB data to CDF file. Details on the specification and containing of the CDF file can be found in [AD-2].

5 Description of the output data

5.1 Output time span

One data file for each Swarm-AEBS product is produced per Swarm satellite (Alpha, Bravo, or Charlie). The Swarm-AEBS product series consists of a total of five products. Two Swarm-AEBS products, *AEJxLPL_2F* and *AEJxLPS_2F*, come as daily files. Three Swarm-AEBS products, *AEJxPBL_2F*, *AEJxPBS_2F* and *AOBxFAC_2F*, come as annual files that are updated on a daily basis.

Daily and annual files are produced only when the corresponding Level 1b (L1b), L2, and/or model files for the given satellite and date are available. Detailed description of the output variables including type, description, and units can be found in [AD-2].

5.2 Quality flagging of PBS and PBL

The table below describes the quality flagging of *AEJxPBL_2F* and *AEJxPBS_2F* products, more detailed information can be found in [AD-2]. Her, the analysis area is defined as the following: QD latitudes from 50° to 85° (Northern hemisphere) or -50° to -85° (Southern hemisphere). Note that Swarm orbits does not always cover this area completely.

Value	Meaning
0000000000000	Both EEJ and WEJ are detected, and their current densities are zero at all boundaries.
0000000000001	No eastward currents detected.
0000000000010	No westward currents detected.
000000000100	Equatorward EEJ boundary occurs at the edge of the analysis area, and the density is larger than 20% of peak value.
000000001000	Poleward EEJ boundary occurs at the edge of the analysis area, and the density is larger than 20% of peak value.
000000010000	Equatorward WEJ boundary occurs at the edge of the analysis area, and the density is larger than 20% of peak value.
000000100000	Poleward WEJ boundary occurs at the edge of the analysis area, and the density is larger than 20% of peak value.
000001000000	Swarm orbit does not fully cover the predefined oval latitude range. Latitude gap is 2 degrees or larger.
000010000000	Equatorward EEJ boundary occurs at the edge of the analysis area.
000010000000	Poleward EEJ boundary occurs at the edge of the analysis area.
000100000000	Equatorward WEJ boundary occurs at the edge of the analysis area.
001000000000	Poleward WEJ boundary occurs at the edge of the analysis area.
010000000000	Peak value of EEJ occurs at the edge of the analysis area.
100000000000	Peak value of WEJ occurs at the edge of the analysis area.

5.3 Occasional gaps in LPS when plotted according to latitude

When searching the peaks and boundaries of electrojets, the horizontal current density either by SECS or by LC is considered as a function of the QD latitude. Latitude sequences of positive (eastward) and negative (westward) current densities are first detected. The exact begin and end latitudes of a sequence are determined by the interpolated zero-crossings of the current density curve. Next the total current across each sequence is calculated. The eastward electrojet (EEJ) is defined to be located within the sequence of the maximum positive total current, and the westward electrojet (WEJ) is defined to be located within the sequence of the maximum negative total current.

The analysis area for peaks and boundaries in its maximum extent is a predefined QD latitude range from 50° to 85° (northern hemisphere) or from -85° to -50° (southern hemisphere). Since Swarm's orbit does not always cover this completely, the area can be smaller. In practice, Swarm seems to reach always QD $\pm 50^\circ$ but it does not always reach the highest latitudes. The user is warned about this situation with the quality flags if the gap is larger than 2 degrees.

It happens frequently that one or more electrojet boundaries occur at the edge of the analysis area, and the current density is non-zero there. Separate flags indicate whether its magnitude is larger than 20% of the peak value. If this is the case then quite a substantial part of the electrojet remains outside of the analysis area.

In LPS a gap can appear when plotting the products according to latitude. Such situation is related to orbits that do not reach $\pm 85^\circ$ in QD latitude. The reason for a gap is related to the difference between the QD and SECS coordinate systems. The SECS method uses spherical coordinates with a common pole with QD, but QD is not spherical. Our modelling method requires that the SECS latitude is purely increasing or decreasing during an oval crossing. To satisfy this condition, we must sometimes ignore a few points close to the poleward edge.